Applied Nanoscience (2020) 10:3057–3074
https://doi.org/10.1007/s13204-020-01382-2

ORIGINAL ARTICLE

Green synthesis of zinc oxide nanoparticles from the leaf, stem and in vitro grown callus of *Mussaenda frondosa* L.: characterization and their applications

Manasa Dogganal Jayappa[1,2] · Chandrashekar Konambi Ramaiah[1,3] · Masineni Allapuramaiah Pavan Kumar[4,5,6] · Doddavenkatanna Suresh[4] · Ashwini Prabhu[3] · Rekha Punchappady Devasya[3] · Sana Sheikh[1,7]

Received: 21 January 2019 / Accepted: 28 March 2020 / Published online: 9 April 2020

Abstract

Biosynthesis of zinc oxide nanoparticles (ZnO-NPs) was achieved by utilizing the reducing and capping potential of leaf, stem and callus aqueous extracts of *Mussaenda frondosa.*The bioreduced ZnO-NPs were characterized using powder X-ray diffraction (XRD), ultraviolet–visible spectroscopy (UV–Vis spectroscopy), scanning electron microscopy (SEM), energy dispersive spectroscopy (EDS), fourier transform infrared spectroscopy (FTIR) and dynamic light scattering (DLS) techniques. UV–visible spectra of ZnO-NPs showed a strong absorption peak at 370, 376 and 373 nm corresponding to the band gap energy of 3.33, 3.27 and 3.30 eV for ZnO-NPs obtained from leaf (L-ZnO-NP), stem (S-ZnO-NP) and callus (C-ZnO-NP) aqueous extracts, respectively. XRD analysis confirmed the formation of hexagonal wurtzite structures having an average grain size between 5 and 20 nm in diameter. FTIR spectra revealed the presence of stretching vibrations of –O–H, C–H, C–N, C = O groups involved in reduction and stabilization of nanoparticles. SEM images recognize the presence of spongy, spherical, porous agglomerated nanoparticles. DLS analysis and zeta potential values validated the stability of ZnO-NPs. The present investigation puts light on the photocatalytic activity and biological (antioxidant, anti-inflammatory, antidiabetic, antimicrobial, anticancerous) applications of ZnO-NPs. The current study is an attempt to describe an effective, simple and eco-friendly method of ZnO-NP synthesis and to evaluate its potential for various industrial and medical applications.

Keywords Zinc oxide nanoparticle · Antioxidant · Antidiabetic · Antimicrobial · Anticancer · Photocatalytic activity

Introduction

In modern days, ZnO semiconductors have received enormous attention due to their distinct and desirable applications in diverse areas of chemistry, physics, biology, medicine, electronics, etc. These characteristics may be endowed due to their large surface area, reduced size, availability of

Electronic supplementary material The online version of this article (https://doi.org/10.1007/s13204-020-01382-2) contains supplementary material, which is available to authorized users.

✉ Chandrashekar Konambi Ramaiah
profkrchandrashekar@gmail.com

[1] Department of Applied Botany, Mangalore University, Mangalagangothri, Mangalore, Karnataka 574199, India

[2] Department of Studies in Botany, Davangere University, Shivagangothri, Davangere, Karnataka 577007, India

[3] Yenepoya Research Centre, Yenepoya (Deemed to be University), Mangalore, Karnataka 575 018, India

[4] Department of Studies and Research in Biochemistry, Tumkur University, Tumkur, Karnataka 572 103, India

[5] Department of Studies in Biochemistry, Jnana Kaveri PG Centre, Chikka Aluvara, Mangalore University, Mangalore, Karnataka, India

[6] Acharya Institute of Graduate Studies, Soladevanahalli, Bengaluru, Karnataka 560 107, India

[7] St Aloysius College (Autonomous), Mangalore, Karnataka 575003, India

surface specific binding site, catalytic, electronic and thermal properties (Shoeb et al. 2013). ZnO-NPs are commercially available in the form of powders or dispersions, which are extensively used in calamine lotion, baby powders, ceramics, UV filters, ointments, paints, food additives, etc. (Kolodziejczak-Radzimska and Jesionowski 2014). ZnO-NPs have also been reported to possess potential human health benefits such as antimicrobial (Das et al. 2013), antioxidant (Premanathan et al. 2011), anticorrosive (Ansari et al. 2011) and anticancer activity (Li et al. 2010a, b). ZnO belongs to II–VI semiconductor, since it is found in the second and sixth group of the periodic table, with a wide band gap energy of 3.3 eV. Such obvious multifunctional ZnO-NPs have been synthesized by various methods such as precipitation, hydrothermal, sol–gel, electrodeposition and chemical methods (Ramimoghadam et al. 2013). These methods yield ZnO-NPs with diversified distinct morphology, size, shape with an ability to persuade various properties and applications (Yu et al 2005; Macmanus-driscoll 2017). Many of these methods are tedious, exorbitant and utilize toxic chemicals imposing environmental and biological risks. Hence, there is an increasing need for an alternative method of synthesis which is safe, eco-friendly and cost-effective. Green synthesis is an unconventional method of nanoparticle synthesis, which is an eco-friendly, risk-free, inexpensive, hypoallergic, single step synthesis method getting wide attention.

Solution combustion synthesis (SCS) is an extensively used expeditious, safe, facile method for the synthesis of nano-sized metal oxides. SCS is a self-propagating exothermic reaction operating at a high temperature, which employs an aqueous solution comprising a metal nitrate precursor (oxidizing agent) and a combustible fuel (plant extract) (Suresh et al. 2015). The reaction is accompanied with the extensive release of gases, yielding highly porous, thin, homogenous, nanosized, crystalline nanoparticles (Rajeshwar and Tacconi 2009).

Mussaenda frondosa L. is an important medicinal plant belonging to the family Rubiaceae. Crude extract of the plant contains important bioactive principles: phenols, flavonoids, alkaloids, steroids, glycosides, tannins, etc. (Manasa et al. 2017). From time immemorial, the herbal preparations of this plant were extensively used in the treatment of asthma, fever, cough, leprosy, wounds, jaundice and so on (Kirtikar and Basu 1987). Due to the presence of highly valuable and medicinal bioactive principles, the plant is overexploited for its medicinal applications.

In vitro culturing such as callus and suspension cultures seems to be a promising alternative for the use of microbes or field-grown plant parts, since these cultures are easily renewable resources generated axenically without generating hazardous by-products. In vitro regenerated callus cultures do not require repeated subculturing like microbial cultures. Till date, very few reports are available on the biosynthesis of nanomaterials through callus cultures (Satyavani et al. 2011; Iyer et al. 2016).

The current study deals with the synthesis of ZnO-NPs via SCS method using aqueous extracts of leaf, stem and in vitro grown (leaf derived) callus of *M. frondosa*. as a combustible fuel. The synthesized nanoparticles were characterized (XRD, UV–Vis, SEM, EDS, FTIR and DLS) and studied for biomedical applications, using theirantioxidant, antimicrobial, anti-inflammatory, antidiabetic and anticancer activities.

Materials and methods

Materials

Healthy leaf and stem parts of *M. frondosa* were collected from natural forests of Dakshina Kannada (12.8158° N and 74.9241° E), Karnataka, India. The plant was authenticated by Flora of Madras Presidency (Gamble 1958) and a voucher specimen (No: MU/AB/DJM-02) was deposited in the Dept. of Applied Botany, Mangalore University. 1, 1-dipheny l-2-picrylhydrazyl (DPPH), α-amylase, starch and DNS were procured from Sigma-Aldrich. Methanol, zinc nitrate hexahydrate [Zn $(NO_3)_2{\cdot}6H_2O$] and methylene blue dye were procured from S.D. Fine chemicals. Murashige and Skoog medium (MS Media) and growth regulators were purchased from Hi-media (India). α-Glucosidase and p-nitrophenyl-beta-D-glucoside (P-PNPG) were purchased from SRL.

Induction, proliferation and preparation of callus samples

The surface sterilization and establishment of callus cultures were carried out from the leaf explants of *M. frondosa* (Manasa et al. 2017). The healthy, friable callus was obtained from the MS medium supplemented with 1-naphthalene acetic acid (NAA) + kinetin (Kn) (2 + 4 mg/l). The obtained callus was subcultured once in 30 days, and consequently harvested after the fourth subculturing. The harvested callus was repeatedly washed with sterile distilled water (dH_2O), dried in a hot air oven for 45 days (at 35 °C), ground into fine powder using mortar and pestle, packed in airtight polyethylene bags and stored in a refrigerator (4 °C) until further use.

Preparation of leaf, stem and leaf-derived callus extract

M. frondosa leaf and stem samples were washed with sterile dH_2O, dried under shade, powdered and stored at 4 °C.

The plant material (leaf, stem and leaf derived callus) and distilled water in the ratio of 1:10 was taken in a round bottom flask and the extraction was carried out at 100 °C under reflux for 4 h. The extract was filtered through Whatmann filter paper No. 1 and centrifuged to remove any undissolved debris. The extract was reduced to 1/5 volume using flash evaporator and stored in airtight bottles at 4 °C.

Biofabrication of ZnO-NPs

ZnO-NPs were prepared by SCS method using aqueous extracts of callus, leaf and stem according to Nethravathi et al. (2015). Two grams of plant extract was dissolved in 100 ml dH_2O with continuous stirring on a magnetic stirrer (450 to 500 rpm) for about 15 min. The stoichiometric amount of Zn $(NO_3)_2{\cdot}6H_2O$ was dispersed in a known amount of combustible fuel to make a reaction mixture and kept in a preheated muffle furnace for combustion at 400 °C for 10–30 min.

Morphological and structural characterization of nanoparticles

The crystalline structure and phase purity were analyzed by XRD (Shimadzu-7000) using CuK_α (1.541 Å) radiation with a nickel filter operating at a voltage of 50 kV and a current of 30 mA (2θ ranging between 20° and 80°). UV–Vis spectrophotometer (Evolution-220, ThermoScientific) was used to examine the optical properties at a resolution of 1 nm in a wavelength range of 280–800 nm. The size, shape and surface morphology were studied by FESEM (Carl Zeiss FESEM) with 10 kV acceleration voltages. For SEM analysis, the samples were placed on carbon-coated tape, air dried and then used for imaging. The elemental composition of synthesized NPs was analyzed using EDS attached to SEM. Functional groups present in the sample were recorded by FTIR (AIM-8800) analysis under the spectral range of 4000–400 cm^{-1} with a resolution of 4 cm^{-1}. Size distribution, size measurement, stability, surface charge and an average zeta potential of NPs in the suspension were determined using Microtrac (USA) particle size analyzer. The samples were dispersed in sterile dH_2O, sonicated for 30 min and then subjected to DLS analysis. All the experiments were carried out thrice and the data were analyzed using Origin 8 software.

Photocatalytic activity

Photocatalytic degradation of methylene blue dye was performed in a 150 × 75 mm batch reactor according to Nethravathi et al. (2015). A catalytic load of 20 mg (ZnO-NPs) was added to 100 ml of methylene blue (5 ppm) dye. The pH (7) was maintained by adding 0.05 M NaOH or 0.05 M H_2SO_4. The sludge consisting of dye and catalyst was placed in the batch reactor and stirred magnetically for agitation with instantaneous exposure to UV light. The noted volume of the sludge was withdrawn at various time points, viz., 10, 20, 30, 40 and 50 min, centrifuged at 6000 rpm for 15 min and absorbance was recorded using UV–Vis spectrophotometer at 660 nm to determine the rate of degradation. The percentage degradation of methylene blue dye was determined using the following equation:

$$\%\ \text{Degradation} = \frac{C_\text{i} - C_\text{f}}{C_\text{i}} \times 100,$$

where C_i is the initial concentration of the methylene blue dye. C_f is the final concentration of the methylene blue dye.

Antioxidant activity

The antioxidant activity of ZnO-NPs was analyzed by DPPH radical scavenging assay as reported by Kumar et al. (2015) with minor modifications. DPPH is a stable free radical and a well-known trap ("scavenger") for other radicals. DPPH radical has deep purple color in solution due to the strong absorption band centered at about 520 nm, and it becomes colorless or pale yellow when neutralized by accepting an electron from the antioxidant molecule. This nature allows visual observation of the reaction, due to change in the optical absorption at 520 nm or in the EPR (electron spin resonance) signal of the DPPH. A concentration of 0.14 mM of DPPH was prepared by dissolving 39.4 mg of DPPH in 100 ml of methanol. Varying concentrations of nanoparticles (2–20 mg) were mixed with 50% methanol and 140 µl of 0.14 mM DPPH solution was added. The mixture was incubated for 30 min at room temperature (dark condition) and the absorbance was recorded at 520 nm using spectrophotometer (Evolution-220, ThermoScientific) against the blank solution (50% methanol). Ascorbic acid was used as a reference standard for measuring the scavenging activity. The actual absorbance was taken as the absorbance difference of the control and test sample; IC_{50} values were determined. The mixture without test sample was considered as control.

Antimicrobial activity

Antibacterial activity of ZnO-NPs was performed using disc diffusion technique (CLSI 2012) aganist two Gram-positive bacteria, viz., *Staphylococcus aureus* [National Collection of Industrial Microorganisms (NCIM)-2079] and *Bacillus subtilis* [American Type Culture Collection (ATCC)—6633] and three Gram-negative bacteria, viz., *Escherichia coli* (NCIM 2931), *Pseudomonas aeruginosa* (NCIM 2200) and *Proteus vulgaris* (NCIM 2813) procured from National Chemical Laboratory, Pune, India. Bacterial strains were grown on

nutrient broth (NB) at 37 °C. The bacterial inoculum was prepared by subculturing the organism on the NB and incubated at 37 °C overnight. Hundred microliters (1×10^6 cfu/ml) of an overnight grown culture of bacteria was inoculated into an autoclaved NB and incubated for 4–5 h at 37 °C.

Twenty milliliters of sterilized Muller Hilton agar was dispensed into sterile petri plates and allowed for solidification. 100 µl of microbial inocula (containing 1×10^6 cfu/ml) was spread on the plates. Sterile antimicrobial susceptibility filter paper discs (6 mm in diameter-Himedia Lab) loaded with 20 µl of the extract/ZnO-NPs (10 mg/ml) were placed on swabbed plates. Streptomycin sulfate (10 mg/ml) was used as a positive control and sterile dH_20 as a negative control. Bacterial growth inhibition was recorded by measuring the zone of inhibition around the discs. The experiment was carried out thrice and the mean values were tabulated.

Minimum inhibitory concentration (MIC)

The MIC of ZnO-NPs was determined by macrobroth dilution method in NB (CLSI 2012). Each bacterial strain (24 h old cultures) were 100-fold diluted in NB by adding bacterial inoculums (100 µl) into broth (10 ml) to obtain 10^6 cfu/ml of bacteria. Further, the broth was poured into separate test tubes. Stock solutions (10 mg/ml) of nanoparticle wee prepared in sterile dH_2O. Varying concentrations (12.5, 25, 50, 100 and 200 µg/ml) of ZnO-NPs were added to the test tubes containing bacterial cultures and incubated at 37 °C for 24 h. Negative (only broth without nanoparticles) and positive control tubes (standard drug streptomycin) were maintained during the experiments. Observations were made for visual turbidity before and after incubation for 24 h. The turbidity of the sample was assessed by measuring the absorbance at 630 nm.

Anti-inflammatory activity

The anti-inflammatory activity of ZnO-NPs (100–500 µg/ml) was assessed using human red blood cells membrane stabilization method (HRBCsMS) according to Shinde et al. (1999) with slight modifications. Blood samples were collected from healthy human volunteers who had not taken non-steroidal anti-inflammatory drugs (NSAIDs) for 2 weeks before the experiment. The blood was mixed with an equal volume of Alsever's solution (2% dextrose, 0.8% sodium citrate, 0.5% citric acid and 0.42% sodium chloride) and centrifuged (3, 000 rpm) for 5 min. The packed cells were washed with isosaline (0.85% at pH 7.21), and a final concentration of 10% v/v suspension was prepared. Different concentrations of ZnO-NPs were prepared to which, 1 ml of phosphate buffer (0.15 M at pH 7.4), 2 ml of hyposaline (0.36%) and 0.5 ml of HRBC suspensions were added. The suspension was incubated at 37 °C (30 min) and centrifuged at 3,000 rpm (3 min). The spectroscopic measurement of the supernatant was recorded at 560 nm to determine the content of hemoglobin. The positive (diclofenac sodium) and negative controls (without the nanoparticles) were maintained during the experiment. The percentage inhibition of hemolysis was determined using the following equation:

$$\%\text{inhibition of hemolysis} = \frac{\text{Abs of control} - \text{Abs of sample}}{\text{Abs of control}} \times 100,$$

where Abs is absorbance at 560 nm.

In vitro antidiabetic activity

α-Amylase inhibitory activity

The α-amylase inhibitory assay was determined using Kim et al.'s (2005) method. The activity was carried out in a 96-well microplate. The reaction mixture in each well containing 50 µl phosphate buffer (50 mM, pH = 5.8), 50 µl α-amylase (16 U/mg) and 20 µl of varying concentrations of ZnO-NPs (Test) was dispersed in buffer (100, 200, 300, 400 and 500 µg/ml) and preincubated at room temperature (RT) for 10 min. To this mixture, 50 µl of soluble starch (1%) in 50 mM phosphate buffer (pH 5.8) was added and incubated for 10 min at RT. Acarbose at varying concentrations (100–500 µg/ml) was used as a standard. The α-amylase activity was determined by recording the absorbance values at 405 nm using a microplate reader (Synergy H1 BIOTEK). Blank contains only buffer and negative control is a mixture without the test sample. The results were expressed as percentage inhibition, which was calculated using the following equation:

$$\text{Inhibitory activity } (\%) = \left(1 - A_t/A_c\right) \times 100,$$

where A_t is the absorbance of the test sample and A_c is the absorbance of the control. IC_{50} values were calculated by using percentage inhibitory activities.

α-Glucosidase inhibitory activity

α-Glucosidase inhibitory activity of ZnO-NPs was determined according to Sanap et al. (2010) with slight modification. In a 96-well plate, the reaction mixture containing 50 µl phosphate buffer (0.3 mM, pH = 6.8), 40 µl alpha-glucosidase (1 U/ml), and 20 µl of varying concentrations of ZnO-NPs (100, 200, 300, 400 and 500 µg/ml) was preincubated at 37 °C for 10 min. Further, 40 µl of 2 mM P-NPG was added to the mixture and incubated at 37 °C for 10 min. The reaction was stopped by adding 0.2 M Na_2CO_3 (70 µl). The absorbance was recorded using a microplate reader (Synergy H1 BIOTEK) at 405 nm to determine the release

of p-nitrophenol. Acarbose at various concentrations (100–500 µg/ml) was used as a standard. Buffer alone was used as a blank, and the well without the test sample was set as a negative control. Each experiment was carried out in triplicate. The results were expressed as percentage inhibition of α-glucosidase activity using the following equation:

$$\text{Inhibitory activity } (\%) = \left(1 - A_t/A_c\right) \times 100,$$

where A_t is the absorbance of test, A_c is the absorbance of the control and IC_{50} values were obtained using percentage inhibitory activities.

Anticancer activity

Cells and culture conditions

Human lung adenocarcinoma cells (A549) were procured from the National Centre for Cell Sciences (NCCS), Pune. They were cultured in Dulbecco's modified Eagle's medium (DMEM) supplemented with 10% fetal bovine serum and 1% antibiotic–antimycotic solution (Himedia, India). They were incubated at 37 °C under 5% CO_2, subcultured upon attaining 70% confluence and used for the experiments after three consecutive passages.

Cytotoxicity assessment using methyl thiazolyl tetrazolium (MTT) assay

The cytotoxicity of the ZnO-NPs on A549 cells was evaluated using the MTT assay (Mosmann 1983). Cells were seeded at a density of 5000 cells/well in 96-well microtiter plates and incubated at 37 °C under 5% CO_2 in a humidified atmosphere for 24 h. Nanoparticles were dispersed in culture medium (10 mg/ml) and then sonicated in an ultrasonicator for 1 h. The solution was then diluted with medium to different concentrations of 12.5, 25, 50, 100 and 200 µg/ml and vigorously vortexed for 30 s prior to cell exposure to avoid nanoparticle agglomeration. ZnO-NPs were added to the cells at concentrations of 12.5, 25, 50, 100 and 200 µg/ml and incubated further for 48 h. 100 µl of MTT solution (1 mg/ml) was added to the wells and incubated for 4 h. Formazan crystals were solubilized in dimethyl sulfoxide (DMSO) and the absorbance was recorded at 570 nm using multimode microplate reader (FluoSTAR Omega, BMG Labtech). The percentage of cell viability was determined using the following equation:

$$\text{Percentage of cell viability} = (\text{Absorbance of control} - \text{Absorbance of test}/\text{Absorbance of control}) \times 100.$$

IC_{50} was calculated using a percentage of cell viability.

Apoptosis detection by acridine orange–ethidium bromide (AO–EB) staining

AO–EB staining was performed to detect the apoptosis (Azizi et al. 2017). AO and EB are DNA-specific dyes which can differentiate dead cells from viable cells. Upon disintegration of the cell membrane, AO can penetrate into both live and dead cells, while EB can intrude into dead cells only. Therefore, AO-stained cells appear green in color (live cells); EB stains dead cells, imparting a greenish yellow to red color during the early and late stages of apoptosis. A549 cells were seeded onto six-well plates at a density of 5000 cells/well and incubated at 37 °C for 24 h under 5% CO_2. ZnO-NPs were added to the cells at their IC_{50} concentrations as determined by MTT assay and incubated further for 48 h at 37 °C under 5% CO_2. The spent media were removed, and cells were fixed in chilled methanol at RT for 20 min. Further, methanol was removed and the cells were stained with a mixture of AO and EB stain and incubated at 37 °C in dark for 15 min. The cells were washed with phosphate buffer saline (PBS) to remove the excess stain. Cells were overlaid with PBS (1 ml) and photographed using fluorescent imager (ZOE, BioRad) to detect the nuclear changes.

Statistical analysis

All the experiments were carried out thrice (n = 3). The experimental data were analyzed by SPSS statistical package software version 20 with Duncan's multiple range test grouping.

Results and discussion

Biogenic synthesis of ZnO-NPs

A milky white, voluminous and foamy powder was formed after 10–15 min, which indicated the formation of ZnO-NPs. The experiment was repeated with 5, 10, 15, 20, 25 and 30 ml of leaf, stem and callus extracts, respectively. The resultant foamy powder was milled using mortar and pestle; stored in airtight containers and kept in dessicators for further use.

Morphological and structural characterization of nanoparticles

Powder XRD

Powder XRD is the primary characterization tool for the nanoparticles. The typical XRD patterns of the resultant ZnO-NPs with different concentrations of leaf (L-ZnO-NP), stem (S-ZnO-NP) and callus (C-ZnO-NP) extracts are represented in Fig. 1 a, b and c. The spectra confirmed the presence of hexagonal wurtzite crystal structure, wherein each Zn^{+2} ion is ordered in a tetragonal coordination with a polar symmetry throughout the hexagonal axis, attributing to its distinctive properties. All the diffraction peaks matched with the Joint Committee on Powder Diffraction Standards (JCPDS) card no 036-1451 and the plots corresponded to the hexagonal wurtzite structure (Suresh et al. 2015). No other impurity peaks were observed in the plots. The average particle size was recorded using the Scherer's equation:

$$D = \frac{0.89\lambda}{\beta \mathrm{Cos}\theta}$$

where D is the crystallite size, β is the full width at half maximum, θ is the diffraction angle and λ is the wavelength of X-rays.

The peaks in the plots seem to be broadening, indicating that the particles in the prepared material are in the nanoscale. XRD shows the diffraction peaks at $2\theta = 31.77°$, 34.40°, 36.22°, 47.61°, 56.58°, 62.85° and 67.93°

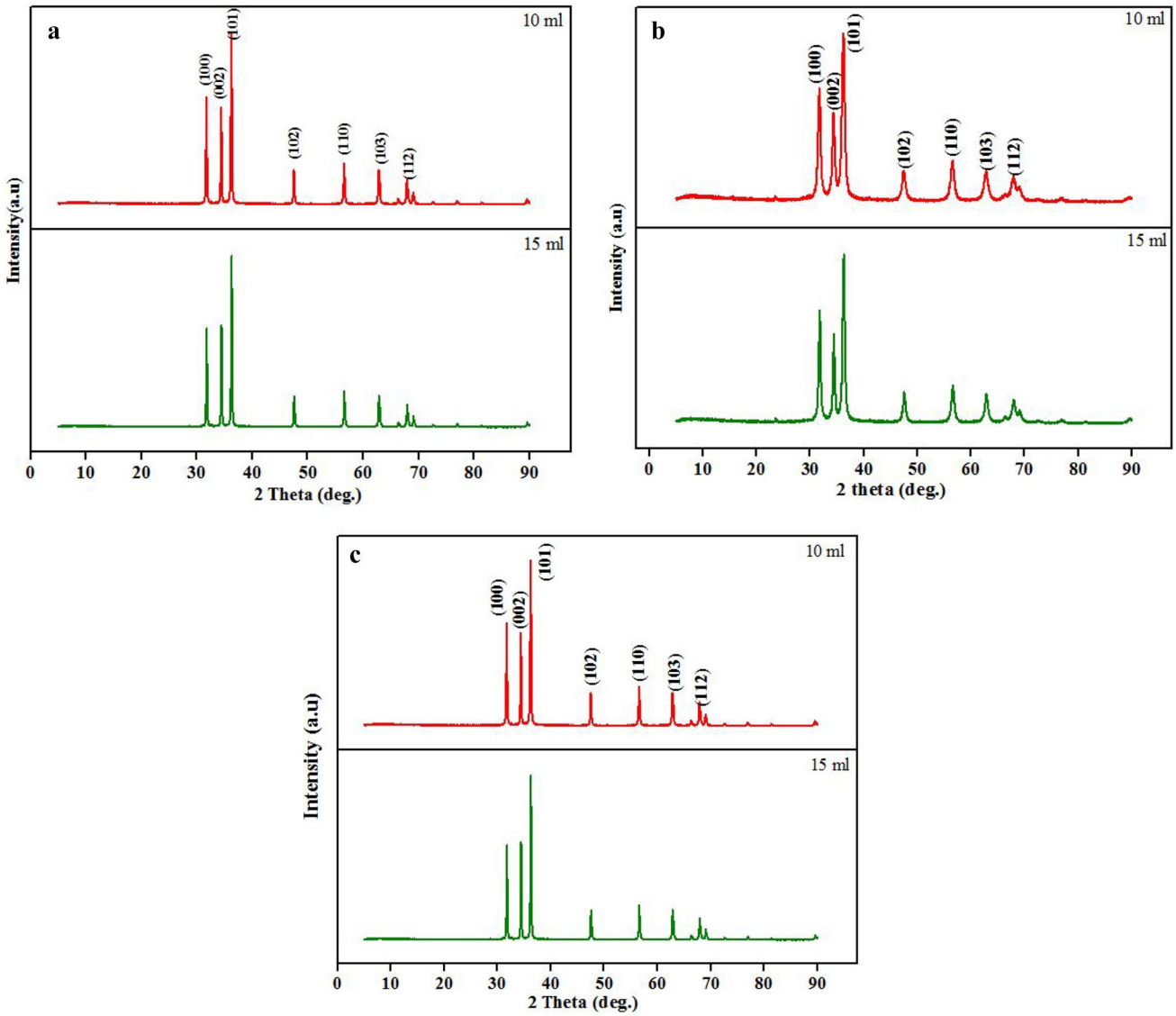

Fig. 1 Diffraction pattern of ZnO-NPs synthesized from different parts of *M. frondosa*. **a** L-ZnO-NP, **b** S-ZnO-NP and **c** C-ZnO-NP

corresponding to (100), (002), (101), (102), (110), (103) and (112) planes, confirming the formation of pure wurtzite structure of ZnO-NPs, respectively (Bala et al. 2015). The crystallite size obtained using 10 and 15 ml of extracts was found to be 8 and 15 nm (L-ZnO-NP); 9 and 12 nm (S-ZnO-NP); 5 and 7 nm (C-ZnO-NP) respectively. The reaction of metal nitrate with the fuel greatly influenced the particle size as observed in XRD images. The results confirmed the more or less similar crystalline structure of L-ZnO-NP, S-ZnO-NP and C-ZnO-NP, but differ in crystallite size.

UV–Vis spectra

The UV–Vis absorption spectra revealed a characteristic maximum absorbance at 370 nm (L-ZnO-NP), 376 nm (S-ZnO-NP) and 373 nm (C-ZnO-NP) corresponding to a bandgap of 3.33, 3.27 and 3.30 eV respectively (Fig. 2), which could be due to intrinsic bandgap absorption of ZnO and electron transitions from the valence band to the conduction band as observed by Zak et al. (2012). The band gap (E_g) of bulk ZnO material ($E_g = 3.45148$ eV) was greater than the estimated bandgap of the synthesized ZnO-NPs because of the effective size of the nanoparticles. Sharp peaks in the absorption spectra imply that the particles are nanosized with narrow particle size distribution. The peak was shifted away from origin when compared to the bulk, indicating the red shift due to quantum size effects (Xu et al. 2004).

This red shift can be explained by the formation of narrow levels inside the bandgap due to impure atoms existing in the lattice. Quantum size effects on electronic energy bands of semiconductors become more prominent when the size of the nano-crystallites is less than the bulk exciton

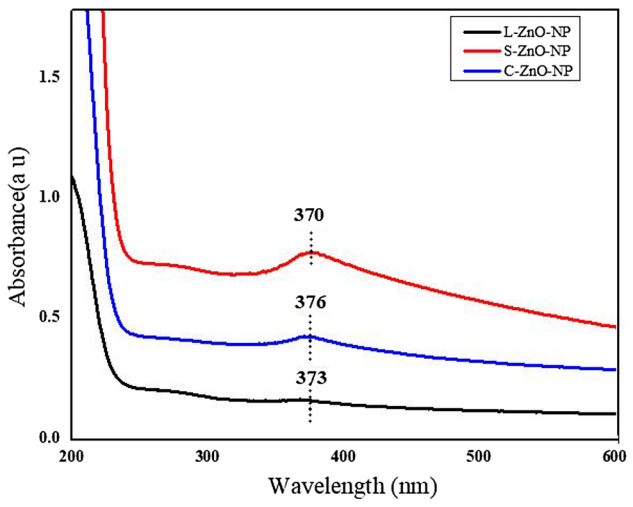

Fig. 2 UV–visible spectra of ZnO-NPs synthesized from different parts of and *M. frondosa*. **a** L-ZnO-NP, **b** S-ZnO-NP and **c** C-ZnO-NP

Bohr radius. Coulomb interactions between holes and electrons play a crucial role in nano sized solids. The quantum confinement of charge carriers modifies valence and conduction bands of semiconductors. The band gap was calculated from the absorption spectrum using the following equation (Tauc 1966);

$$\alpha h\nu = D\left(h\nu - E_g\right)^n,$$

where h is the energy of the photon, E_g is the band gap of the material and D is a constant. The transition data provides the best linear fit in the banded region for $n = 1/2$.

SEM imaging and EDS analysis

SEM imaging of L-ZnO-NP (Fig. 3a, b) showed the flaky agglomerated hexagonal structures wheras, C-ZnO-NP (Fig. 3e, f) and S-ZnO-NP (Fig. 3c, d) showed high density spherical shaped nanoparticles with pores resulting from the escape of gases during combustion synthesis. Similar observations were made by Geetha et al. (2016) and Karnan and Selvakumar (2016) from ZnO-NPs synthesized from *Euphorbia jatropa* and *Nephelium lappaceum* respectively. Aggregation could be due to a high surface energy of ZnO-NPs and also perhaps due to densification as an outcome of narrow space between nanoparticles.

EDS spectra revealed the presence of three peaks between 1 and 10 keV confirming the presence of Zinc with a strong peak at 1 keV (Fig. 4) (Bala et al. 2015). Oxygen and Zinc are present at a stoichiometric ratio of 20: 80, indicating the absence of impurity peaks. The presence of carbon in the spectra might be due to the presence of stabilizing agents from the plant extract which probably acted as a capping agent for the synthesized nanoparticles. Various reports have been found that the peak of Zn in EDS spectra appears to be around the same region (Raj and Jayalakshmy 2015; Joel and Badhusha 2016).

FTIR spectroscopy

Plant extracts exhibited various functional group stretches between 3350 cm^{-1} and 1045 cm^{-1} (Fig. 5). Extracts of leaf, stem and callus of *M. frondosa* showed characteristic absorption peaks at 3350, 2922, 2344, 1580, 1377 and 1045 cm^{-1} corresponding to OH stretching of intra-molecular hydrogen bond, C–H stretching of alkanes, –N–H stretching of amide in proteins, –P–H stretching of phosphines, C=O stretching of carboxylic acids and C–N stretching vibrations of aliphatic and aromatic amines respectively. Shifting of these following peaks were observed in FTIR spectra of nanoparticles such as 2922 to 2913, 2344 to 2352, 1580 to 1690, 1377 to 1529 cm^{-1} inferring the role of these functional groups in the bioreduction and stabilization of ZnO-NPs.

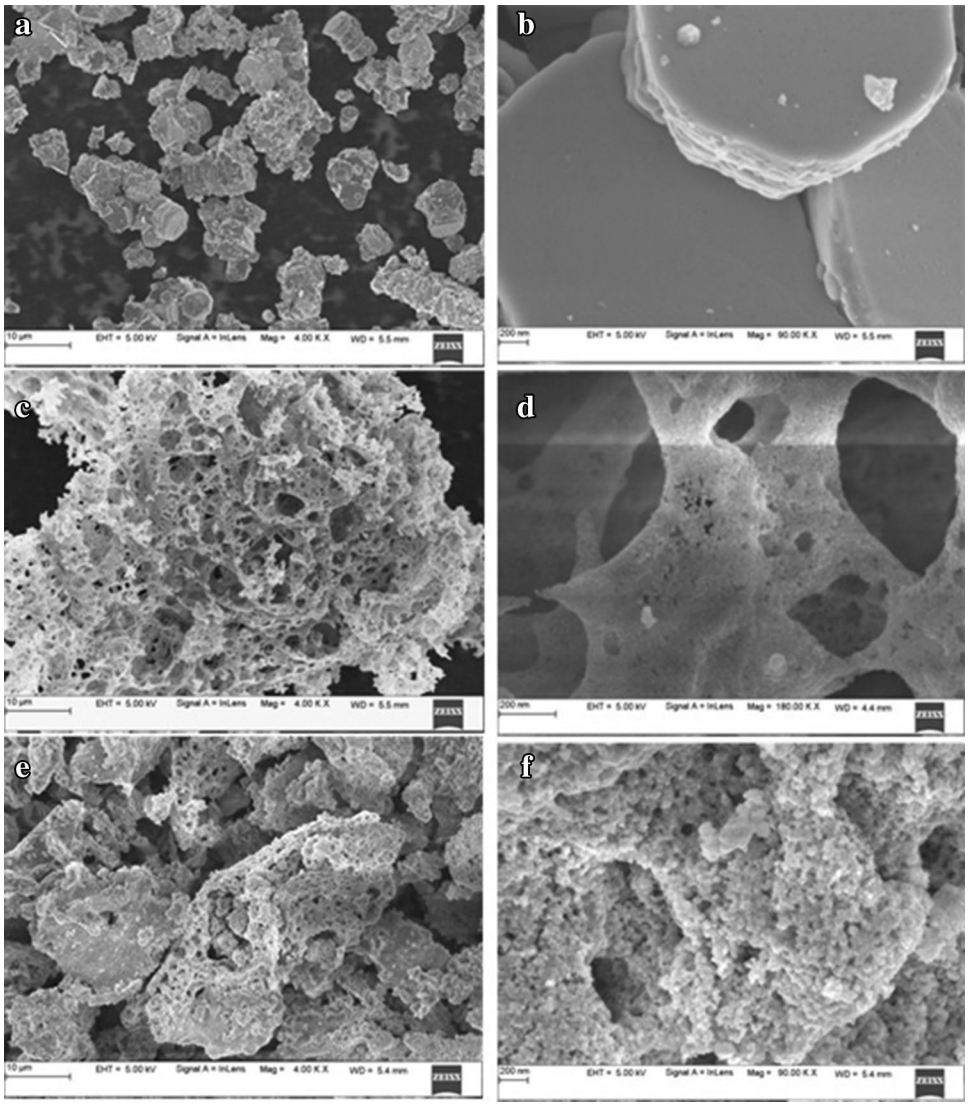

Fig. 3 SEM images of synthesized ZnO-NPs at different magnifications of *M. frondosa*: **a**, **b** L-ZnO-NP, **c**, **d** S-ZnO-NP, **e**, **f** C-ZnO-NP

The absorption peaks at 475 cm^{-1} (L-ZnO-NP), 486 cm^{-1} (S-ZnO-NP) and 473 cm^{-1} (C-ZnO-NP) (Fig. 6) represent the stretching vibrations of metallic ZnO resulting from inter-atomic vibrations. The absence of 3350 cm^{-1} peak in synthesized ZnO-NPs denotes that the material is free from moisture. Further, the FTIR spectra of ZnO-NPs showed the disappearance of the 1045 cm^{-1} peak indicates that the functional group complex well to form metallic oxide nanoparticle. The obtained results were in aggreement with Sangeeta et al. (2011), Bhuyan et al. (2015) and Murali et al. (2017).

DLS analysis

DLS is an extensively used technique for determining the hydrodynamic diameter of nanoparticles established on the brownian movement of particles in the suspension. The average hydrodynamic size of the nanoparticles (Fig. 7) calculated by DLS is quite larger than the theoretical size of the nanoparticles calculated using XRD (Jamdagni et al. 2018). The variation in the nanoparticle size could be associated with the polydispersity Index (PDI) values in turn related to the existence of nanoparticles as aggregates or agglomerates. PDI measurements were found to be > 0.7 indicated the monodispersion and homogeneity of the nanoparticles in the medium except for C-ZnO-NP (PDI = 0.895) showing slight polydispersity (Table 1). The Zeta potential values of the synthesized NPs was found to be 11.0, − 25.4 and − 17.7 mV for L-ZnO-NP, S-ZnO-NP and C-ZnO-NP respectively confirming the synthesized NPs are highly stable (Table 1). Customarily, the zeta potential values between + 30 and − 30 mV results in a stable colloidal formulation (Murali et al. 2017).

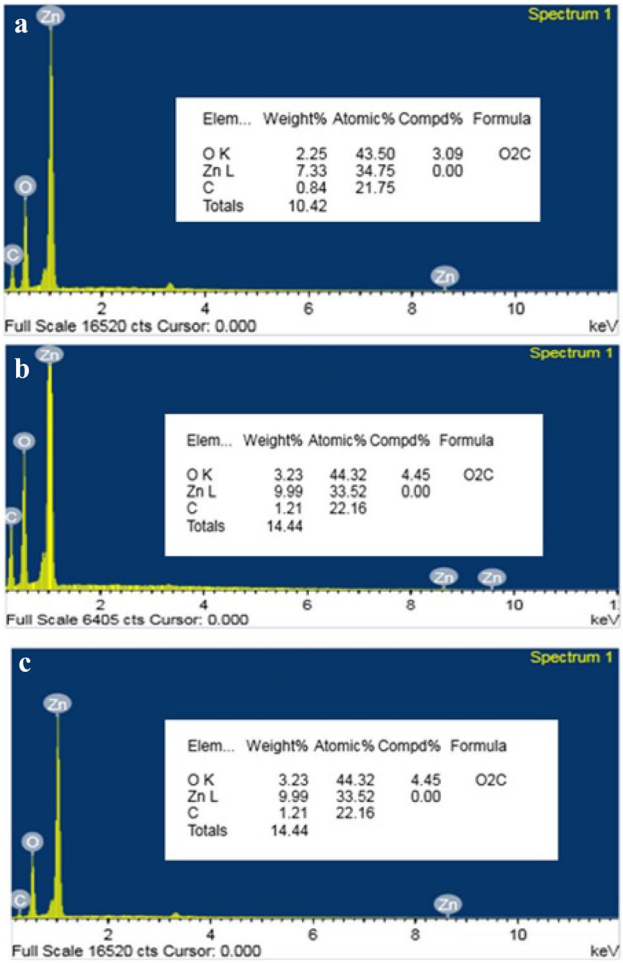

Fig. 4 EDS spectra of ZnO-NPs from *M. frondosa*. **a** L-ZnO-NP, **b** S-ZnO-NP and **c** C-ZnO-NPs

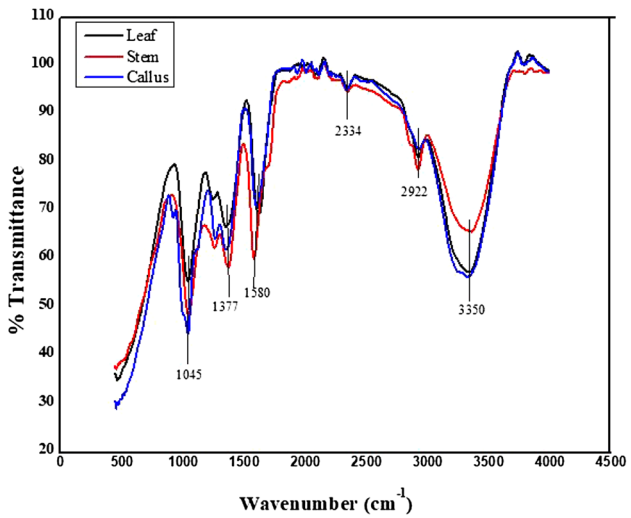

Fig. 5 FTIR Spectra of aqueous extracts of *M. frondosa*

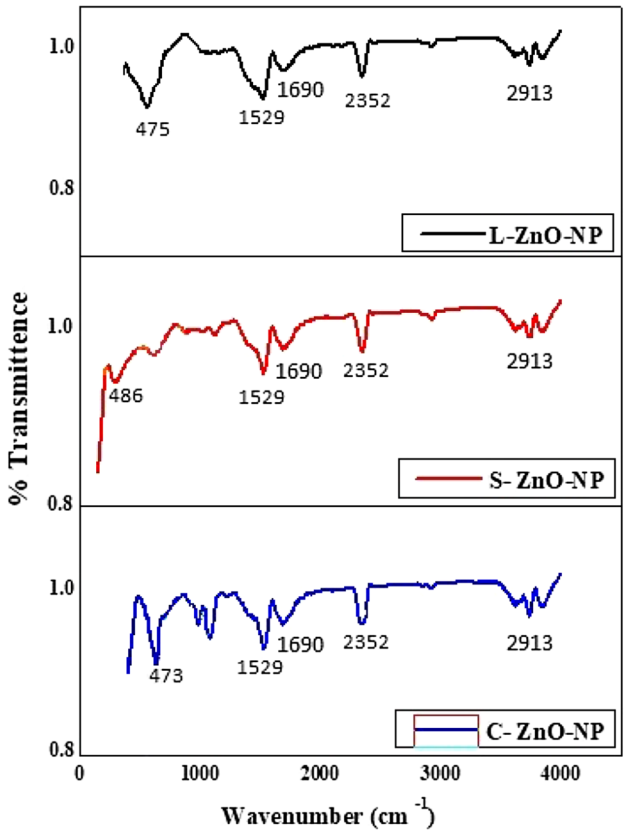

Fig. 6 FTIR Spectra of *M. frondosa* ZnO-NPs

Photocatalytic activity

In the present study, it was observed that about 30% (L-ZnO-NP), 30% (S-ZnO-NP) and 90% (C-ZnO-NP) of the methylene blue dye was degraded in the presence of UV light at a time duration of 100, 100 and 120 min respectively (Fig. 8). The biofabricated ZnO-NPs were used for the degradation of carcinogen organic dyes as a photocatalyst; ascribed to its composition, particle size, crystallinity, a band gap of the photocatalyst, surface area etc. ZnO-NPs prepared from *M. frondosa* plant extracts were used as a catalyst because of their better bulkiness, purity and high yield. The photodegradation efficiency does not soley depend on UV irradiance, but also determined on the intensity of light, a concentration of O_2, OH^- (Soltani and Entezari 2013).

The mechanism of photodegradation is that upon UV irradiation semiconductors (catalyst) absorbs the energy (photon) higher than their band gap energy leads to charge separation due to jumping of an electron from the valence band to the conduction band of the catalyst, thus a hole is generated in the valence band. The created holes bring about the oxidation of water; as a consequence a highly reactive unstable $OH^{\cdot}$ radical is generated ultimately leading the degradation of dyes.

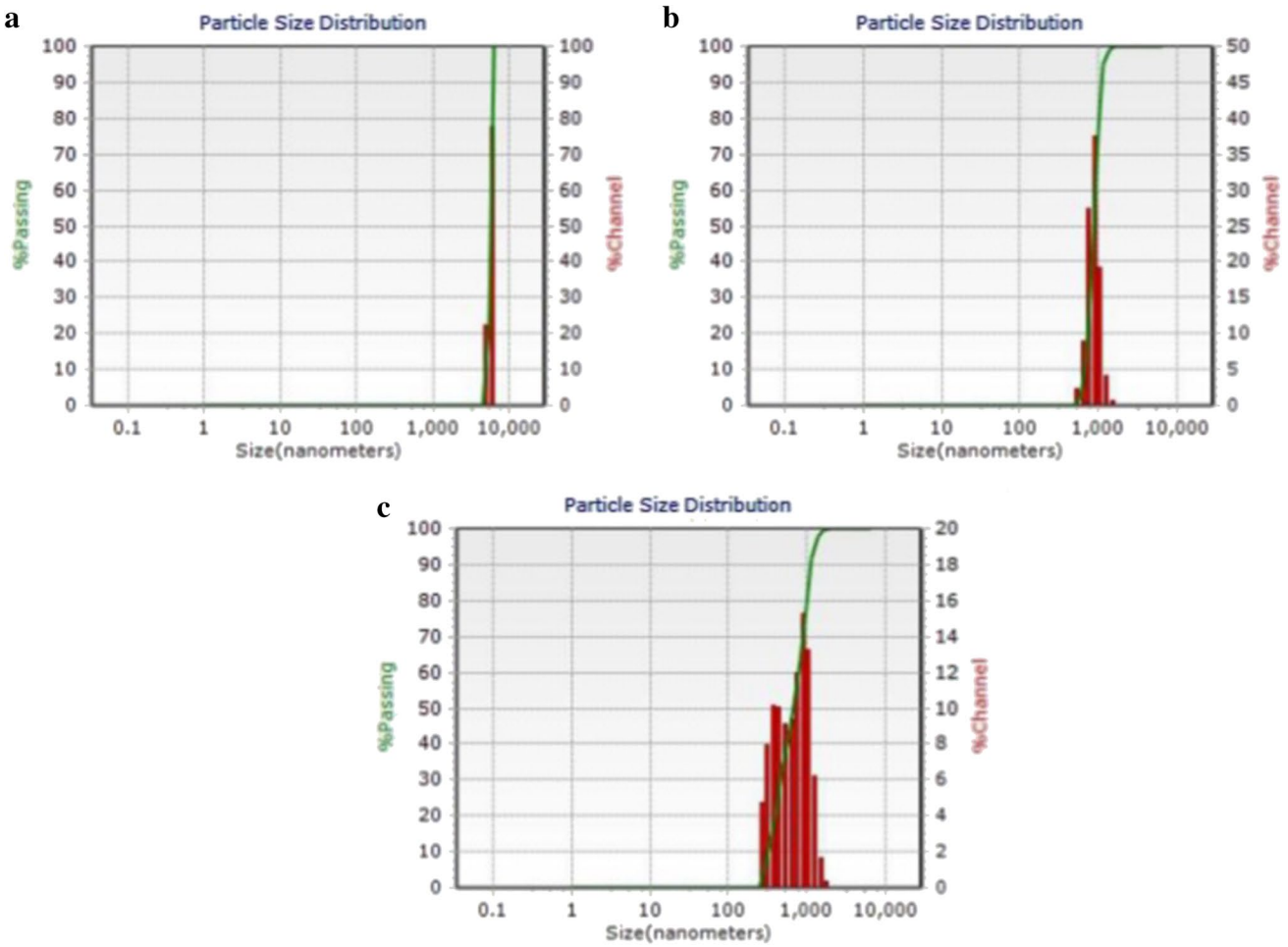

Fig. 7 DLS analysis of ZnO-NPs from *M. frondosa.* **a** L-ZnO-NP, **b** S-ZnO-NP and **c** C-ZnO-NP

Table 1 Zeta potential and PDI values of the ZnO-NPs synthesized from different parts of *M. frondosa*

Sample	Zeta potential values (mV)	Polydispersity index (PDI)
L-ZnO-NP	11	0.041
S-ZnO-NP	− 25.4	0.506
C-ZnO-NP	− 17.7	0.895

Antioxidant activity

DPPH molecule is categorized as a stable free radical by the virtue of delocalization of free electron over the whole molecule so that the molecules do not dimerize imparting deep violet color. This was characterized by an absorption band centered at about 515 to 520 nm in 50% methanol solution. When 0.14 mM DPPH is added to the solution containing

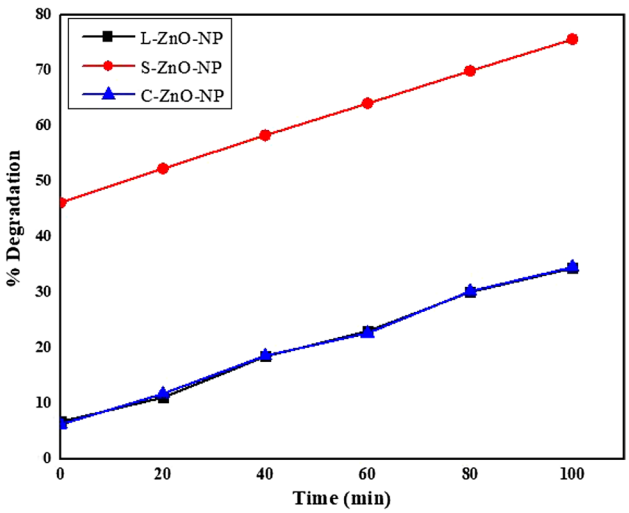

Fig. 8 Methylene blue dye elimination by ZnO-NPs under UV light

nanoparticles, the nanoparticles can donate an electron to DPPH, which gets oxidized to give yellow colored solution

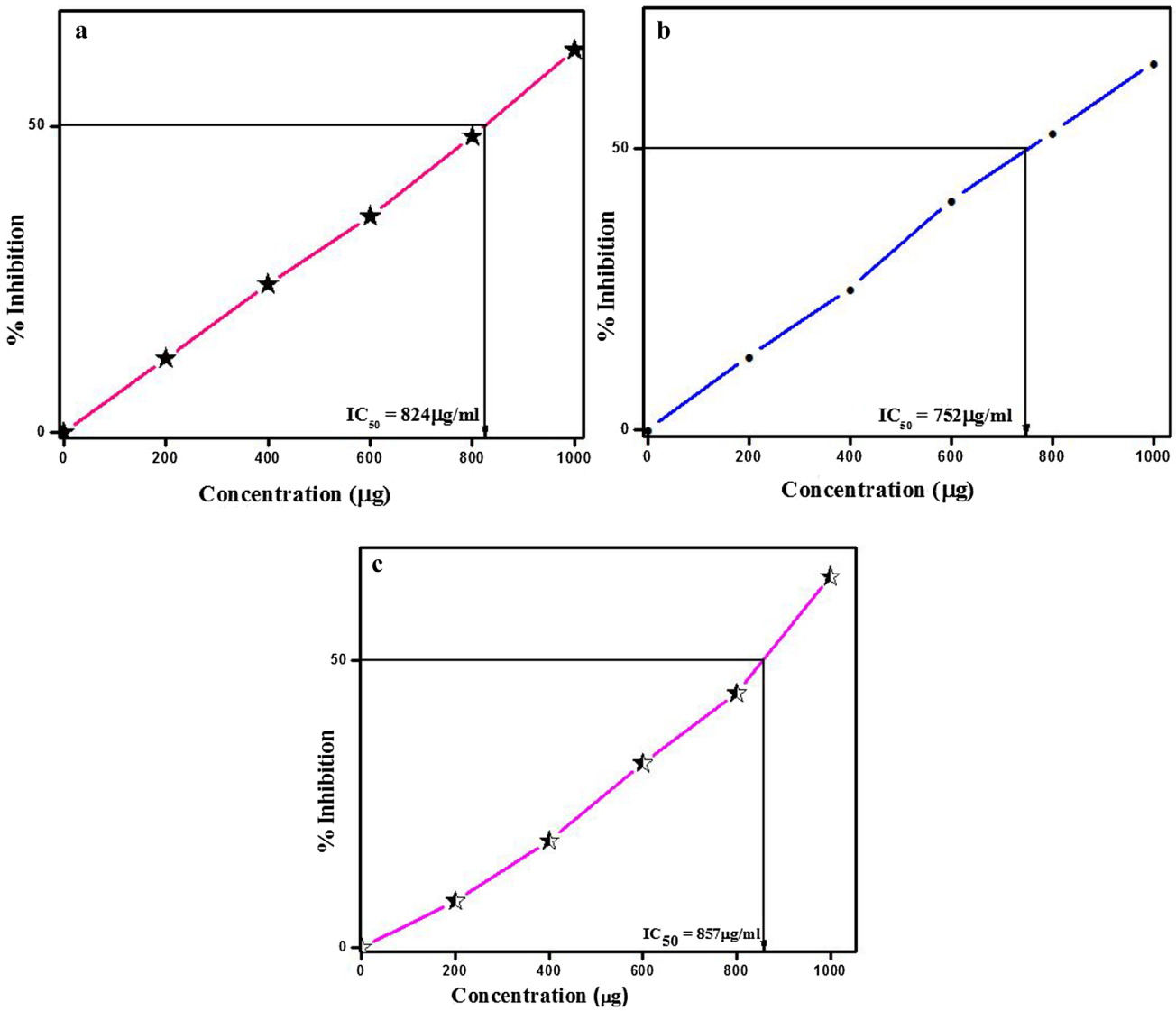

Fig. 9 DPPH radical scavenging activity of ZnO-NPs synthesized from *M. frondosa*. **a** L-ZnO-NP, **b** S-ZnO-NP, **c** C-ZnO-NP

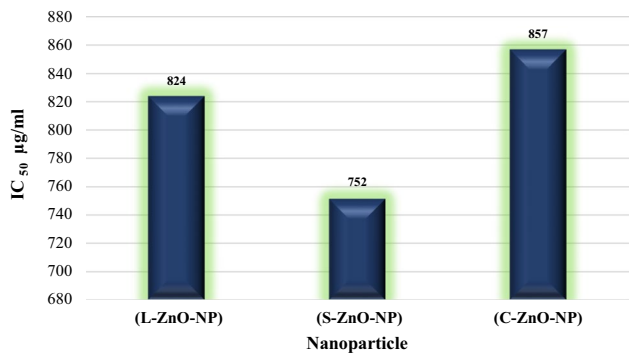

Fig. 10 DPPH radical scavenging activity of ZnO-NPs synthesized from *M. frondosa*

(Kanipandian et al. 2014). Thus the DPPH molecule represents the free radicals formed in the system whose activity is to be suppressed by the substance and the antioxidant potential of ZnO-NPs was assessed through DPPH.

The IC_{50} value of ZnO-NPs for quenching DDPH radical was found to be 824 µg/ml (L-ZnO-NP), 752 µg/ml (S-ZnO-NP) and 857 µg/ml (C-ZnO-NP) (Fig. 9a–c). The S-ZnO-NP exhibited effective antioxidant activity compared to L-ZnO-NP and C-ZnO-NP (Fig. 10). The antioxidant activity is due to the electrostatic attraction between bioactive compounds (COO^-) and ZnO ($ZnO = Zn^{2+} + O^{2-}$) of *M. frondosa* (Kumar et al. 2010). Phenolic compounds and flavonoids associated with *M. frondosa* have the ability to quench free radical owing to its antioxidant activity (Manasa et al. 2017). Kumar et al. (2015) is also of the opinion that the nanoparticles that

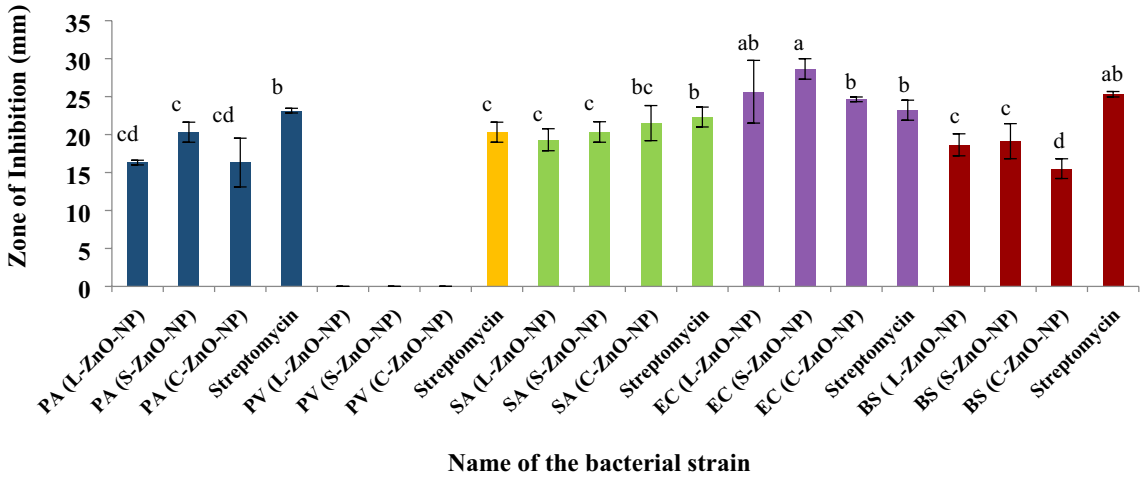

Fig. 11 Antimicriobial activity of ZnO-NPs of *M. frondosa.* PA: *Pseudomonas aeruginosa*, BS: *Bacillus subtilis,* SA: *Staphylococcus aureus*, EC: *Escherichia coli*, PV: *Proteus vulgaris*

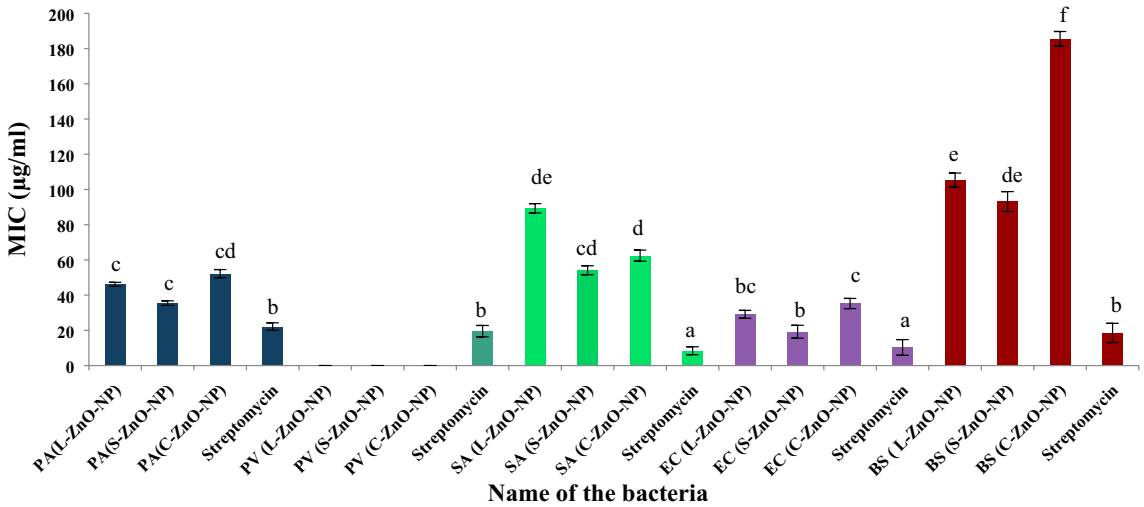

Fig. 12 MIC values of ZnO-NPs of *M. frondose.* PA: *Pseudomonas aeruginosa*, BS: *Bacillus subtilis,* SA: *Staphylococcus aureus*, EC: *Escherichia coli*, PV: *Proteus vulgaris*

the nanoparticles showed considerable antioxidant activity for quenching the free radical scavenging of DPPH.

Antimicrobial activity

The results of growth inhibition (in mm) against the tested bacterial strains are depicted in Fig. 11, 12 and 13. It was observed that all the ZnO-NPs showed inhibition against all the tested strains except *P.vulgaris.* Among the tested strains, *E.coli* was found to be more susceptible to S-ZnO-NPs with 28.64 mm zone of inhibition ($p < 0.05$) compared to standard and other samples. No inhibition of growth was observed in bulk ZnO, sterile dH_2O and aqueous plant extracts against all the tested bacterial strains (Fig. 13). The highest mean zone of inhibition observed against *P. aeruginosa*, *S. aureus* and *B. subtilis* was found to be 20.31 mm (S-ZnO-NP), 21.51 mm (C-ZnO-NP) and 19.13 mm (S-ZnO-NP) respectively at $p < 0.05$. These results are in agreement with the findings of Mahendra et al. (2017), wherein the greater antibacterial efficiency was observed in green synthesized ZnO-NPs rather than the plant extracts of *Cochlospermum religiosum* (L.). Similarly, the antimicrobial activity of the *Allophylus serratus* leaf extract mediated silver nanoparticles (Ag-NPs) exhibited more activity than the *Allophylus serratus* callus extract mediated Ag-NPs (Jemal et al. 2017) which is in accordance with the present findings.

The amplified bioactivity of these nanoscale particles may be due to the higher surface area to volume ratio, size

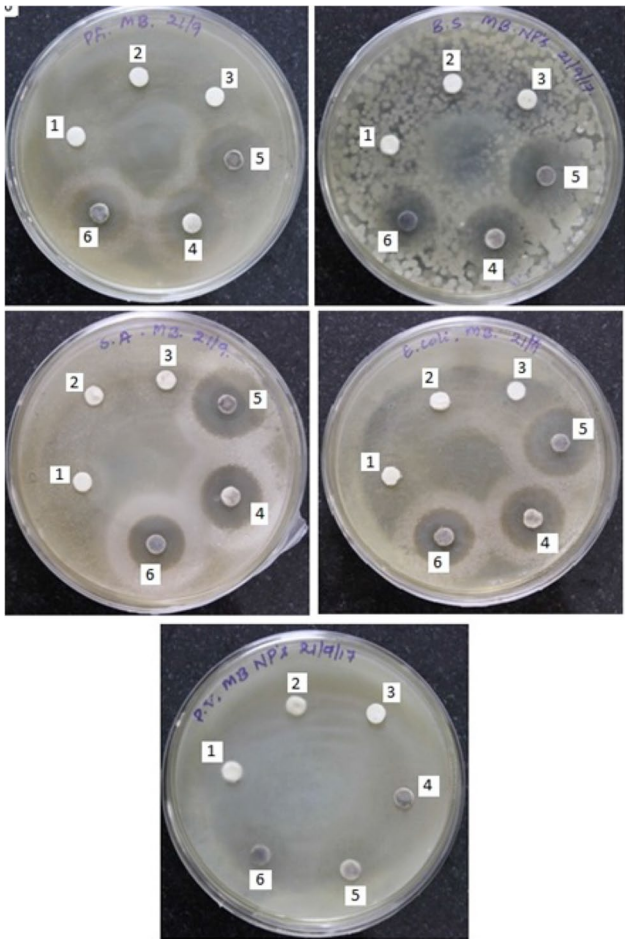

Fig. 13 Antimicrobial activity of ZnO-NPs. PA: *Pseudomonas aeruginosa*, BS: *Bacillus subtilis,* SA: *Staphylococcus aureus*, EC: *Escherichia coli*, PV: *Proteus vulgaris*, 1 mixture of aqueous extracts of leaf, stem and callus, 2 zinc oxide—bulk, 3 sterile distilled water, 4 L-ZnO-NPs, 5 S-ZnO-NPs, 6 C-ZnO-NPs

of the particles, morphology and larger band gap of the nanoparticles. Toxicity might be due to the increase in H_2O_2 molecules on the surface of ZnO-NPs, which can induce oxidative stress in bacterial cell membranes, in turn affecting the membrane permeability and eventually leading to inhibition of cell growth, finally causing the death of cells (Elumalai and Velmurugan 2015). The efficiency of antibacterial activity increased with a decrease in the particle size from bulk ZnO to green synthesized white ZnO-NPs, implying that antibacterial activity is inversely proportional to the size of the metallic oxides (Raghupathi et al. 2011).

MIC

Highly significant MIC was recorded against *E.coli* at 19.23 µg/ml at $p < 0.05$, which was followed by the maximum activity against *P. aeruginosa, S. aureus, B. subtilis* showing MIC values of 35.46, 54.13 and 93.14 µg/ml by S-ZnO-NPs of *M. frondosa* (Fig. 12). Similar results were reported from ZnO-NPs synthesized from the aqueous leaf extract of *Cochlospermum religiosum* (L.), wherein microbicidal efficacy was noted in the range of 4.8 to 625 µg/ml (Mahendra et al. 2017). Streptomycin showed the least MIC of 8.44 µg/ml against *S. aureus*, followed by 10.31, 18.54, 19.54 and 22.13 µg/ml against *E. coli*, *B. subtilis*, *P.vulgaris* and *P. aeruginosa*, respectively. The MIC values of the standard (8.44 to 22.13 µg/ml) were slightly higher than that of the biosynthesized ZnO-NPs (19.23–185.54 µg/ml). The overall microbicidal efficacy was moderately higher in S-ZnO-NPs against all the bacterial strains tested, which might be due to its smaller particle size, well-dispersed particles and voluminous yield compared L-ZnO-NP and C-ZnO-NPs.

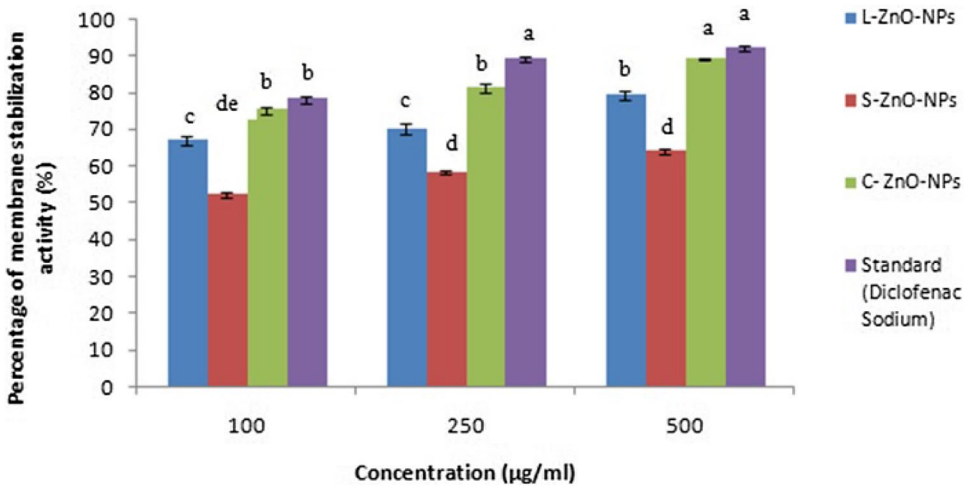

Fig. 14 Anti-inflammatory activity of ZnO-NPs by HRBC-sMS method. Values are the mean of three replicates ± SD. Means with the same letters in the same column showed insignificant difference ($P \leq 0.05$)

Anti-inflammatory activity

Green synthesized ZnO-NPs exhibited varying degrees of membrane stabilizing activity in a dose-dependent manner (Fig. 14). The percentage protection of L-ZnO-NP, S-ZnO-NP and C-ZnO-NP showed activity in a range between 67.16 to 79.13%, 52.14 to 64.13% and 75.16 to 89.31%, respectively. Hence, C-ZnO-NPs exhibited highly significant activity (89.31% at 500 µg/ml) at $p < 0.05$ which is on par with the standard drug (92.16% at 500 µg/ml). Ali et al. (2017) also reported 89% membrane stabilization at 2000 µg/ml by ZnO-NPs, which was on par with the standard drug aspirin. Our studies reported that the membrane protection method for evaluating in vitro anti-inflammatory activity is due to the similarity between human RBCs membrane and lysosomal membrane, which is in line with the works reported by Bruton (2005) and Di Rosa et al. (1971). The stabilization implies that the biosynthesized ZnO-NPs may efficiently stabilize lysosomal membranes and are biocompatible in nature at lower concentrations.

In vitro antidiabetic activity

α-Amylase inhibition assay

The synthesized ZnO-NPs showed moderate α-amylase inhibitory activity (Fig. 15). L-ZnO-NP ($IC_{50} = 54.33$ µg/ml), S-ZnO-NP ($IC_{50} = 47.66$ µg/ml) and C-ZnO-NP ($IC_{50} = 51.66$ µg/ml) exhibited on par α-amylase inhibitory activity which was comparatively less than that of standard acarbose ($IC_{50} = 35.66$ µg/ml). The antidiabetic potential of biofabricated ZnO-NPs was also justified by Thatoi et al. (2016) who reported IC_{50} values of about 334.40 and 394.38 µg/ml for the ZnO-NPs synthesized using the aqueous extracts of two mangrove plant species, viz., *Heritiera fomes* and *Sonneratia apetala*, respectively.

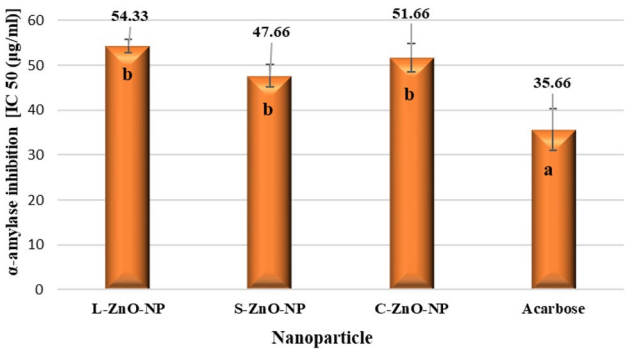

Fig. 15 In vitro α-amylase inhibition study of ZnO-NPs of *M. frondosa*. Values are the mean of three replicates ± SD. Means with different letters indicate significant difference ($P \leq 0.05$)

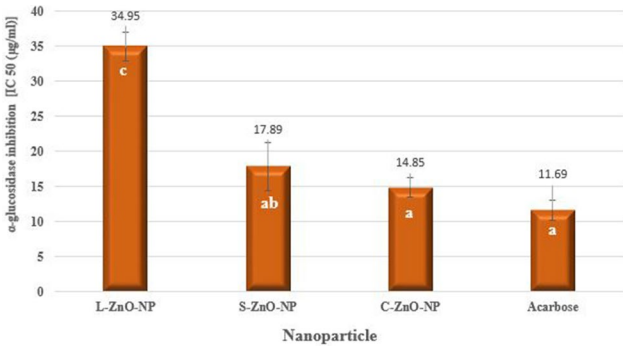

Fig. 16 In vitro α-glucosidase inhibition study of ZnO-NPs of *M. frondosa*. Values are the mean of three replicates ± SD. Means with the same letters in the same column showed insignificant difference ($P \leq 0.05$)

α-Glucosidase inhibition study

ZnO-NPs exhibited moderately good inhibitory activity against α-glucosidase (Fig. 16). C-ZnO-NP (14.85 µg/ml) and acarbose (11.69 µg/ml) displayed on par α-glucosidase inhibitory activity at $p < 0.05$. Kitture et al. (2015) found 61.93% α-glucosidase inhibition by ZnO-NPs synthesized using a plant extract of red sandalwood as a fuel.

Diabetes mellitus is an association of metabolic dysfunction wherein the affected person has uncontrolled blood sugar level. There are certain synthetic drugs and food items which can prevent the disease to certain levels, yet complete treatment is impossible. Therefore, biofabricated ZnO-NPs could be a potent starch blocker drug to cure this dysfunction (Dhobale et al. 2008). The complex polysaccharides and disaccharides in the food are broken down into simple monosaccharides by the enzymes α-amylase and α-glucosidase. The elevated blood sugar level after food intake (postprandial hyperglycemia) could be reduced via inhibiting the activities of these two enzymes eventually reducing carbohydrate hydrolysis. Many of the synthetic drugs rely on this startegy of inhibition with certain side effects such as abdominal bloating and diarrhoea (Kitture et al. 2015; Ghosh et al. 2012). Looking at the above results of α-amylase and α-glucosidase inhibition assays, green synthesized ZnO-NPs could be effectively used as a potent antidiabetic drug which was found to be a stable and biocompatible form of zinc associated with insulin metabolism.

Cytotoxicity studies

An increasing cytotoxicity effect on A549 cells was observed by ZnO-NPs with an increasing concentration of nanoparticles, indicating a dose-dependent action (Fig. 17) which was in accordance with the observations of Akhtar et al. (2012). Results of the MTT assay revealed that C-ZnO-NP and

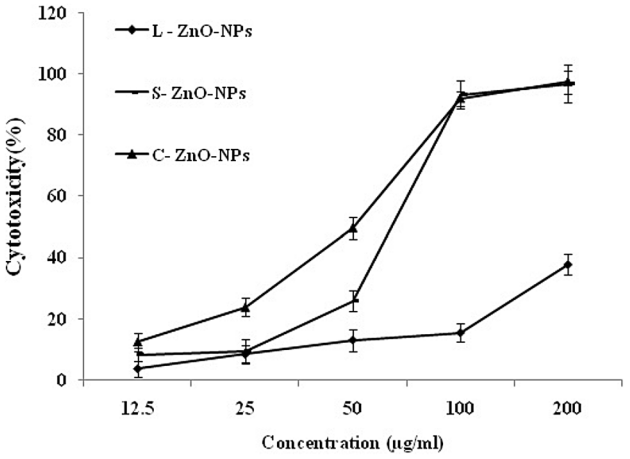

Fig. 17 In vitro cytotoxicity of ZnO-NPs of *M. frondosa.* Values are the mean of three replicates ± SD

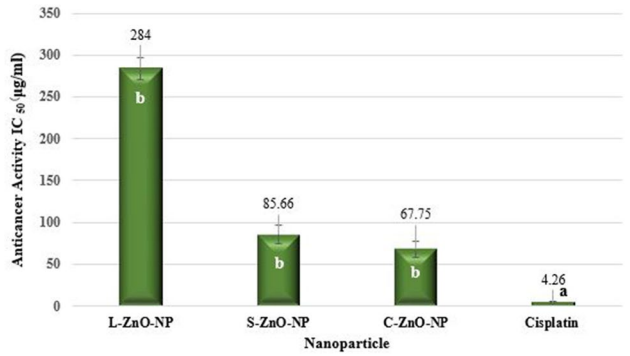

Fig. 18 Anticancer activity (MTT assay) of ZnO-NPs of *M. frondosa.* Values are the mean of three replicates ± SD. Means with the same letters in the same column showed insignificant difference ($P \leq 0.05$)

S-ZnO-NP exhibited on par cytotoxic activity on lung adenocarcinoma cells with an IC_{50} value of 67.75 and 85.66 µg/ml, respectively (Fig. 18). Vijayakumar et al. (2016) reported the anticancer activity of ZnO-NPs synthesized using *Laurus nobilis* leaf extract against A549 cells. C-ZnO-NP showing the lowest IC_{50} value was selected to study the impact of NP against A549 cell lines on morphological and nuclear changes by AO/EB double staining.

AO/EB staining is the most frequently used method for differentiating viable, early apoptotic and late apoptotic cell populations in response to drug treatments (Liu et al. 2015). Untreated control A549 cells stained green indicating the viable cells (Fig. 19c). C-ZnO-NPs exerted a significant cytotoxic activity on the tested lung adenocarcinoma cells. The nuclei of cells treated with C-ZnO-NP were stained red, indicating the late apoptosis, showing the presence of condensed chromatin (Fig. 19a). Cells treated with compound 'cisplatin' (standard), showing late apoptotic cells with condensed chromatin, were stained yellowish orange (Fig. 19b). Our observations are in line with the recent study of Dobrucka and Dlugaszewska (2016), who demonstrated ZnO-NPs synthesized from the extracts of *Trifolium pratense* induced cytotoxicity and apoptosis in human non-small cell lung cancer A549.

Nanoparticles could induce cytotoxicity in cancer cell lines, leading to various consequences such as oxidative stress-induced injury, inflammation associated with the release of proinflammatory mediators, fibrosis and so on. Upon the breakdown of metallic oxide nanoparticles, some of the toxic responses are induced in the cell, which is dangerous to the cell components themselves (Lewinski et al. 2008). Nanosized structures enter the biological system through intravenous, skin, subcutaneous, oral and intraperitoneal means. The entered nanoparticles are absorbed to interact with biological components of cells, such as nucleic acids and proteins, distributing various organs of the body where they will be modified, metabolized or remain structurally same to exhibit their toxicity (Rahban et al. 2010). Sun et al. (2012) proposed a different hypothesis for induced toxicity of nanoparticles, which is autophagy or cellular self-digestion. Many reports had focused attention on the nanoparticles which are novel activators of autophagy and induce autophagy cell death (Chen et al. 2005; Zabirnyk et al. 2007; Li et al. 2010a, b).

The overall results showed that S-ZnO-NPs exhibited the highest photocatalytic, antioxidant, antimicrobial, antidiabetic and anticancer activity compared to L-ZnO-NP and C-ZnO-NP. This shows that the different phytochemicals exhibited by the leaf, stem and callus extracts might have affected the biological properties as well as photocatalytic activity. Menichini et al. (2011) have also evaluated the relationships between the chemical composition of various plant parts and the biological properties exhibited by them.

This is a pioneering work showing that callus developed by in vitro culturing techniques as well as the wild plant parts could be used for the synthesis of ZnO-NPs. As compared to other biological systems used in nanoparticle synthesis, plant and plant-derived products are gaining much interest, because the method is simple, quick and a straight single step process. Analogous to the present work, researchers such as Mude et al. (2009) and Satyavani et al. (2011) had put efforts in synthesizing nanoparticles from callus derived from plants such as *Carica papaya* and *Citrullus colocynthis*, respectively. Adopting callus cultures for the biosynthesis of nanoparticles is extremely a great concept for the reason that calluses are formed under sterile milieu and are suitable for biomedical applications. There is a need for further research to study the molecular mechanisms involved in these biological activities.

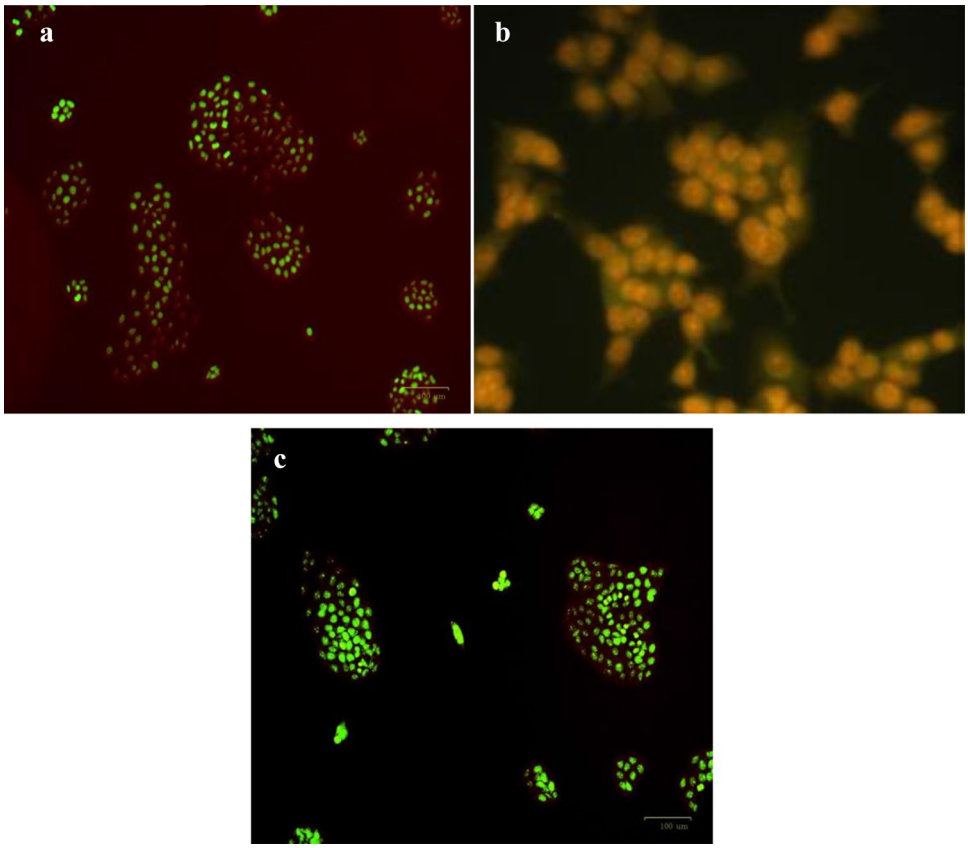

Fig. 19 Acridine orange-ethidium bromide (AO–EB) staining for cell death analysis. **a** Cells treated with compound C-ZnO-NPs, showing late apoptotic cells with condensed chromatin, stained red, **b** cells treated with standard anticancer drug 'cisplatin' showing late apoptotic cells with condensed chromatin, stained yellowish orange, **c** control showing healthy population with intact nulcei, stained green

Conclusion

In summary, multidimensional ZnO-NPs were obtained through leaf, stem and callus extracts of the medicinal plant *M. frondosa* as a fuel, adopting SCS method. This is the first report on the synthesis of ZnO-NPs from callus, leaf and stem extracts of *M. frondosa.* XRD study showed wurtzite structures of ZnO-NPs. The average crystallite size of synthesized semiconductor ZnO-NPs was found in the range of 5-25 nm. The UV–Vis spectral analysis confirmed that the maximum absorption at 370–376 nm range corresponds to the intrinsic band gap of ZnO-NPs. SEM images confirmed the spongy structure of agglomerated spherical-shaped nanoparticles. FTIR spectra revealed the absorption bands between 3350 and 1045 cm^{-1}, confirming the stretching of functional groups involved in the bioreduction of ZnO-NPs. DLS analysis unveiled the monodispersity and stability of bioreduced nanoparticles. Carcinogenic methylene blue dye was efficiently disintegrated using ZnO-NPs under UV light. In addition, the present work also demonstrated a significant antioxidant, anti-inflammatory, antidiabetic and anticancer activities of ZnO-NPs. In brief, this is a simple, effective, biosynthetic method which could be an alternative for chemical and physical methods for the large-scale production of ZnO-NPs. Applications of such eco-friendly ZnO-NPs in different fields such as medicine, catalysis and drug delivery systems make this bioreduction process a highly suitable way for large-scale synthesis.

Acknowledgements The senior author (Manasa. D. J) is thankful to DST (Department of Science and Technology) for awarding INSPIRE fellowship (No: DST/INSPIRE fellowship 2012).

Compliance with ethical standards

Conflict of interest On behalf of all authors, the corresponding author states that there is no conflict of interest.

References

Ali SS, Morsy R, El-Zawawy NA, Fareed MF, Bedaiwy MY (2017) Synthesized zinc peroxide nanoparticles (ZnO2-NPs): a novel antimicrobial, anti-elastase, anti-keratinase, and anti-inflammatory approach toward polymicrobial burn wounds. Int J Nanomed 12:6059–6073. https://doi.org/10.2147/IJN.S141201

Akhtar JM, Ahamed M, Kumar S, Majeed Khan M, Ahmad J, Alrokayan SA (2012) Zinc oxide nanoparticles selectively induce apoptosis in human cancer cells through reactive oxygen species. Int J Nanomed 7:845–857. https://doi.org/10.2147/IJN.S29129

Ansari SA, Husain Q, Qayyum S, Azam A (2011) Designing and surface modification of zinc oxide nanoparticles for biomedical applications. Food Chem Toxicol 49:2107–2115. https://doi.org/10.1016/j.fct.2011.05.025

Azizi M, Ghourchian H, Yazdian F, Dashtestani F, AlizadehZeinabad H (2017) Cytotoxic effect of albumin coated copper nanoparticle on human breast cancer cells of MDA-MB 231. PLoS ONE 12:1–21. https://doi.org/10.1371/journal.pone.0188639

Bala N, Saha S, Chakraborty M, Maiti M, Das S, Basu R, Nandy P (2015) Green synthesis of zinc oxide nanoparticles using *Hibiscus subdariffa* leaf extract: effect of temperature on synthesis, anti-bacterial activity and anti-diabetic activity. RSC Adv 5:4993–5003. https://doi.org/10.1039/C4RA12784F

Bhuyan T, Khanuja M, Sharma R, Patel S, Reddy MR, Anand S, Varma A (2015) A comparative study of pure and copper (Cu)-doped ZnO nanorods for antibacterial and photocatalytic applications with their mechanism of action. J Nanoparticle Res 17:1–11. https://doi.org/10.1007/s11051-015-3093-3

Bruton LL (2005) Goodman and Gilman's pharmacological basis of therapeutics. McGraw-Hill, New York

Chen Y, Yang L, Feng C, Wen LP (2005) Nano neodymium oxide induces massive vacuolization and autophagic cell death in non-small cell lung cancer NCI-H460 cells. Biochem Biophys Res Commun 337:52–60. https://doi.org/10.1016/j.bbrc.2005.09.018

CLSI (2012) Performance standards for antimicrobial disk susceptibility tests; approved standard-eleventh edition. CLSI document M02–A11. Clinical and Laboratory Standards Institute, Wayne.

Das D, Nath BC, Phukon P, Kalita A, Dolui SK (2013) Synthesis of ZnO nanoparticles and evaluation of antioxidant and cytotoxic activity. Colloids Surf B Biointerfaces 111:556–560. https://doi.org/10.1016/j.colsurfb.2013.06.041

Dhobale S, Thite T, Laware SL, Rode CV, Koppikar SJ, Ghanekar R, Kale SN (2008) Zinc oxide nanoparticles as novel alpha-amylase inhibitors zinc oxide nanoparticles as novel alpha-amylase inhibitors. J Appl Phys 104:1–5. https://doi.org/10.1063/1.3009317

Di Rosa M, Giroud JP, Willoughby DA (1971) Studies of the mediators of the acute inflammatory response induced in rats in different sites by carrageenan and turpentine. J Pathol 104:15–29. https://doi.org/10.1002/path.1711040103

Dobrucka R, Dlugaszewska J (2016) Biosynthesis and antibacterial activity of ZnO nanoparticles using *Trifolium pratense* flower extract. Saudi J Biol Sci 23:517–523. https://doi.org/10.1016/j.sjbs.2015.05.016

Elumalai E, Velmurugan S (2015) Green synthesis, characterization and antimicrobial activities of zinc oxide nanoparticles from the leaf extract of *Azadirachta indica* (L.). Appl Surf Sci 345:329–336. https://doi.org/10.1016/j.apsusc.2015.03.176

Gamble JS (1958) Flora of the Presidency of Madras. Botanical Survey of India, Calcutta, India

Geetha MS, Nagabhushana H, Shivananjaiah HN (2016) Green mediated synthesis and characterization of ZnO nanoparticles using *Euphorbia Jatropa* latex as reducing agent. J Sci Adv Mater Devices 1:301–310. https://doi.org/10.1016/j.jsamd.2016.06.015

Ghosh S, Ahire M, Patil S, Jabgunde A, Dusane MB, Joshi BN, Pardesi K, Jachak S, Dhavale DD, Chopade BA (2012) Antidiabetic activity of *Gnidia glauca* and *Dioscorea bulbifera*: potent amylase and glucosidase inhibitors. Evid Based Complement Altern 2012:1–10. https://doi.org/10.1155/2012/929051

Iyer RI, Selvaraju C, Santhiya ST (2016) Biosynthesis of silver nanoparticles by callus cultures of *Vigna radiata*. Indian J Sci Technol 9:1–5. https://doi.org/10.17485/ijst/2015/v9i9/87987

Jamdagni P, Khatri P, Rana JS (2018) Green synthesis of zinc oxide nanoparticles using flower extract of *Nyctanthes arbor-tristis* and their antifungal activity. J King Saud Univ Sci 30:168–175. https://doi.org/10.1016/j.jksus.2016.10.002

Jemal K, Sandeep BV, Pola S (2017) Synthesis, characterization, and evaluation of the antibacterial activity of *Allophylus serratus* leaf and leaf derived callus extracts mediated silver nanoparticles. J Nanomater 2017:1–11. https://doi.org/10.1155/2017/4213275

Joel C, Badhusha MSM (2016) Green synthesis of ZnO nanoparticles using *Phyllanthus embilica* stem extract and their antibacterial activity. Der Pharm Lett 8: 218–223. https://doi.scholarsresearchlibrary.com/archive.html.

Kanipandian N, Kannan S, Ramesh R, Subramanian P, Thirumurugan R (2014) Characterization, antioxidant and cytotoxicity evaluation of green synthesized silver nanoparticles using *Cleistanthus collinus* extract as surface modifier. Mater Res Bull 49:494–502. https://doi.org/10.1016/j.materresbull.2013.09.016

Karnan T, Selvakumar SAS (2016) Biosynthesis of ZnO nanoparticles using rambutan (*Nephelium lappaceum* L.) peel extract and their photocatalytic activity on methyl orange dye. J Mol Struct 1125:358–365. https://doi.org/10.1016/j.molstruc.2016.07.029

Kim YM, Jeong YK, Wang MH, Lee WY, Rhee HI (2005) Inhibitory effect of pine extract on α-glucosidase activity and postprandial hyperglycemia. Nutrition 21:756–761. https://doi.org/10.1016/j.nut.2004.10.014

Kirtikar KR, Basu BD (1987) Indian medicinal plants, 2nd edn. International Book Distributors, Dehradun, pp 2423–2426

Kitture R, Chordiya K, Gaware S, Ghosh S, More PA, Kulkarni P, Chopade BA, Kale SN, Lib C (2015) ZnO nanoparticles-red sandalwood conjugate : a promising anti-diabetic agent. J Nanosci Nanotech 15:4046–4051. https://doi.org/10.1166/jnn.2015.10323

Kolodziejczak-Radzimska JT (2014) Zinc oxide-from synthesis to application: a review. Materials (Basel) 7:2833–2881. https://doi.org/10.3390/ma7042833

Kumar BSA, Lakshman K, Jayaveera KN, Shekar DS, Kumar AA, Manoj B (2010) Antioxidant and antipyretic properties of methanolic extract of *Amaranthus spinosus* leaves. Asian Pac J Trop Med 3:702–706. https://doi.org/10.1016/S1995-7645(10)60169-1

Kumar PMA, Suresh D, Nagabhushana H, Sharma SC (2015) *Beta vulgaris* aided green synthesis of ZnO nanoparticles and their luminescence, photocatalytic and antioxidant properties. Eur Phys J Plus 130:1–7. https://doi.org/10.1140/epjp/i2015-15109-2

Lewinski N, Colvin V, Drezek R (2008) Cytotoxicity of nanopartides. Small 4:26–49. https://doi.org/10.1002/smll.200700595

Li C, Liu H, Sun Y, Wang H, Guo F, Rao S, Deng J, Zhang Y, Miao Y, Guo C, Meng J, Chen X, Li L, Li D, Xu H, Wang H, Li B, Jiang C (2010a) Erratum: PAMAM nanoparticles promote acute lung injury by inducing autophagic cell death through the Akt-TSC2-mTOR signaling pathway. J Mol Cell Biol 2:37–45. https://doi.org/10.1093/jmcb/mjq003

Li J, Guo D, Wang X, Wang H, Jiang H, Chen B (2010b) The photodynamic effect of different size ZnO nanoparticles on cancer cell proliferation in vitro. Nanoscale Res Lett 5:1063–1071. https://doi.org/10.1007/s11671-010-9603-4

Liu K, Park C, Chen H, Hwang J, Bae EY, Lee KW, Kim H, Liu H, Kyun N, Peng C, Jang JH, Kim KE, Ahn JS, Bode AM, Dong Z, Kim BY, Dong Z (2015) Eupafolin suppresses prostate cancer by targeting phosphatidylinositol 3-kinase-mediated Akt signaling. HHS Public Access 54:751–760. https://doi.org/10.1002/mc.22139.Eupafolin

Macmanus-driscoll J (2017) ZnO-nanostructures, defects, and devices. Erschienen Mater Today 7021:40–48. https://doi.org/10.1016/S1369-7021(07)70078-0

Mahendra C, Murali M, Manasa G, Ponnamma P, Abhilash MR, Lakshmeesha TR, Satish A, Amruthesh KN, Sudarshana MS (2017) Antibacterial and antimitotic potential of bio-fabricated zinc oxide nanoparticles of *Cochlospermum religiosum* (L.). Microb Pathog 110:620–629. https://doi.org/10.1016/j.micpath.2017.07.051

Manasa DJ, Chandrashekar KR, Bhagya N (2017) Rapid in vitro callogenesis and phytochemical screening of leaf, stem and leaf callus of *Mussaenda frondosa* Linn.: a medicinal plant. Asian J Pharm Clin Res 10:81–86. https://doi.org/10.22159/ajpcr.2017.v10i6.17527

Menichini F, Loizzo MR, Bonesi M, Conforti F, De Luca D, Statti GA, de Cindio B, Menichini F, Tundis R (2011) Phytochemical profile, antioxidant, anti-inflammatory and hypoglycemic potential of hydroalcoholic extracts from *Citrus medica* L. cv Diamante flowers, leaves and fruits at two maturity stages. Food Chem Toxicol 49:1549–1555. https://doi.org/10.1016/j.fct.2011.03.048

Mosmann T (1983) Rapid colorimetric assay for cellular growth and survival: Application to proliferation and cytotoxicity assays. J Immunol Methods 65:55–63. https://doi.org/10.1016/0022-1759(83)90303-4

Mude N, Ingle A, Gade A, Rai M (2009) Synthesis of silver nanoparticles using callus extract of *Carica papaya*—a first report. J Plant Biochem Biotechnol 18:83–86. https://doi.org/10.1007/BF03263300

Murali M, Mahendra C, Nagabhushan RN, Sudarshana MS, Raveesha KA, Amruthesh KN (2017) Antibacterial and antioxidant properties of biosynthesized zinc oxide nanoparticles from *Ceropegia candelabrum* L.—an endemic species. Spectrochim Acta Part A Mol Biomol Spectrosc 179:104–109. https://doi.org/10.1016/j.saa.2017.02.027

Nethravathi PC, Shruthi GS, Suresh D, Udayabhanu NH, Sharma SC (2015) *Garcinia xanthochymus* mediated green synthesis of ZnO nanoparticles: Photoluminescence, photocatalytic and antioxidant activity studies. Ceram Int 41:8680–8687. https://doi.org/10.1016/j.ceramint.2015.03.084

Premanathan M, Karthikeyan K, Jeyasubramanian K, Manivannan G (2011) Selective toxicity of ZnO nanoparticles toward Gram-positive bacteria and cancer cells by apoptosis through lipid peroxidation. Nanomed Nanotechnol Biol Med 7:184–192. https://doi.org/10.1016/j.nano.2010.10.001

Raghupathi KR, Koodali RT, Manna AC (2011) Size-dependent bacterial growth inhibition and mechanism of antibacterial activity of zinc oxide nanoparticles. Langmuir 27:4020–4028. https://doi.org/10.1021/la104825u

Rahban M, Divsalar A, Saboury AA, Golestani A (2010) Nanotoxicity and spectroscopy studies of silver nanoparticle: calf thymus DNA and K562 as targets. J Phys Chem C 114:5798–5803. https://doi.org/10.1021/jp910656g

Raj LFAA, Jayalakshmy E (2015) Biosynthesis and characterization of zinc oxide nanoparticles using root extract of *Zingiber Officinale*. Orient J Chem 31:51–56. https://doi.org/10.13005/ojc/310105

Rajeshwar K, De Tacconi NR (2009) Solution combustion synthesis of oxide semiconductors for solar energy conversion and environmental remediation. Chem Soc Rev 38:1984–1998. https://doi.org/10.1039/b811238j

Ramimoghadam D, Bin Hussein MZ, Taufiq-Yap YH (2013) Hydrothermal synthesis of zinc oxide nanoparticles using rice as soft biotemplate. Chem Cent J 7:1–10. https://doi.org/10.1186/1752-153X-7-136

Sanap SP, Ghosh S, Jabgunde AM, Pinjari RV, Gejji SP, Singh S, Chopade BA, Dhavale DD (2010) Synthesis, computational study and glycosidase inhibitory activity of polyhydroxylated conidine alkaloids—a bicyclic iminosugar. Org Biomol Chem 8:3307–3315. https://doi.org/10.1039/c004690f

Sangeetha G, Rajeshwari S, Venckatesh R (2011) Green synthesis of zinc oxide nanoparticles by *Aloe barbadensis* Miller. leaf extract: Structure and optical properties. Mater Res Bull 46:2560–2566. https://doi.org/10.1016/j.materresbull.2011.07.046

Satyavani K, Gurudeeban S, Ramanathan T, Balasubramanian T (2011) Biomedical potential of silver nanoparticles synthesized from calli cells of *Citrullus colocynthis* (L.) Schrad. J Nanobiotechnol 9:2–9. https://doi.org/10.1186/1477-3155-9-43

Shinde UA, Phadke AS, Nair AM, Mungantiwar AA, Dikshit VJ, Saraf MN (1999) Membrane stabilizing activity—a possible mechanism of action for the anti-inflammatory activity of *Cedrus deodara* wood oil. Fitoterapia 70:251–257. https://doi.org/10.1016/S0367-326X(99)00030-1

Shoeb M, Singh BR, Khan JA, Khan W, Singh BN, Singh HB, Naqvi AH (2013) ROS-dependent anticandidal activity of zinc oxide nanoparticles synthesized by using egg albumen as a biotemplate. Adv Nat Sci Nanosci Nanotechnol 4:1–11. https://doi.org/10.1088/2043-6262/4/3/035015

Soltani T, Entezari MH (2013) Photolysis and photocatalysis of methylene blue by ferrite bismuth nanoparticles under sunlight irradiation. J Mol Catal A Chem 377:197–203. https://doi.org/10.1016/j.molcata.2013.05.004

Sun T, Yan Y, Zhao Y, Guo F, Jiang C (2012) Copper oxide nanoparticles induce autophagic cell death in a549 cells. PLoS ONE 7:1–7. https://doi.org/10.1371/journal.pone.0043442

Suresh D, Nethravathi PC, Udayabhanu RH, Nagabhushana H, Sharma SC (2015) Green synthesis of multifunctional zinc oxide (ZnO) nanoparticles using *Cassia fistula* plant extract and their photodegradative, antioxidant and antibacterial activities. Mater Sci Semicond Process 31:446–454. https://doi.org/10.1016/j.mssp.2014.12.023

Tauc J (1966) Optical properties of solids. Academic Press, New York

Thatoi P, Kerry RG, Gouda S, Das G, Pramanik K, Thatoi H, Patra JK (2016) Photo-mediated green synthesis of silver and zinc oxide nanoparticles using aqueous extracts of two mangrove plant species, *Heritiera fomes* and *Sonneratia apetala* and investigation of their biomedical applications. J Photochem Photobiol B Biol 163:311–318. https://doi.org/10.1016/j.jphotobiol.2016.07.029

Vijayakumar S, Vaseeharan B, Malaikozhundan B, Shobiya M (2016) *Laurus nobilis* leaf extract mediated green synthesis of ZnO nanoparticles: characterization and biomedical applications. Biomed Pharmacother 84:1213–1222. https://doi.org/10.1016/j.biopha.2016.10.038

Xu PS, Sun YM, Shi CS, Xu FQ (2004) Posttraumatic total dislocation of the upper thoracic spine. Surg Neurol 61:343–346. https://doi.org/10.1016/S0168-583X(02)01425-8

Yu JC, Zhang L, Li SKA (2005) Self-assembly of ZnO nanorods and nanosheets into hollow microhemispheres and microspheres. Adv Mater 17:756–760. https://doi.org/10.1002/adma.200401477

Zabirnyk O, Yezhelyev M, Seleverstov O (2007) Nanoparticles as a novel class of autophagy activators. Autophagy 3:278–281. https://doi.org/10.4161/auto.3916

Zak AK, Yousefi R, Majid WHA, Muhamad MR (2012) Facile synthesis and X-ray peak broadening studies of Zn1xMgxO nanoparticles. Ceram Int 38:2059–2064. https://doi.org/10.1016/j.ceramint.2011.10.042